Chinese Chemical Letters 34 (2023) 107979

Contents lists available at ScienceDirect

Chinese Chemical Letters

journal homepage: www.elsevier.com/locate/cclet

# Tune the photoresponse of monolayer $MoS_2$ by decorating $CsPbBr_3$ perovskite nanoparticles

Chao Tan[a], Rui Tao[a], Zhihao Yang[a], Lei Yang[a], Xiaolei Huang[b], Yong Yang[b], Fei Qi[c], Zegao Wang[a,*]

[a] College of Materials Science and Engineering, Sichuan University, Chengdu 610065, China
[b] State Key Laboratory of Solidification Processing, Center of Advanced Lubrication and Seal Materials, Northwestern Polytechnical University, Xi'an 710072, China
[c] College of Optoelectronic Engineering, Chongqing University of Posts and Telecommunications, Chongqing 400065, China

ARTICLE INFO

*Article history:*
Received 17 September 2022
Revised 29 October 2022
Accepted 2 November 2022
Available online 5 November 2022

*Keywords:*
$MoS_2$ photodetector
$CsPbBr_3$ NPs
Surface charge doping
Carrier mobility
Photoresponse

ABSTRACT

Tuning the photoresponse of monolayer $MoS_2$ could extend its potential application in many fields, however, it is still a challenge. In this study, $CsPbBr_3$ nanoparticles were prepared and spin-coated on the surface of monolayer $MoS_2$ to fabricate hybrid $CsPbBr_3/MoS_2$ photodetectors. By combing the photoelectrical property of the $CsPbBr_3$, the synergistic effect has been systematically studied from its carrier mobility, photoresponse and detectivity. It was found that nanofilm-coating of $CsPbBr_3$ would impede the photoelectric performance due to the electron-hole recombination facilitated by the defects at the interface of $CsPbBr_3$ and $MoS_2$ films. While the nanoparticles decorating was observed to significantly improve the conductivity of the monolayer $MoS_2$, which also increased the on/off ratio of the $MoS_2$ transistor from $8.2 \times 10^3$ to $4.4 \times 10^4$, and enhanced the carrier mobility from 0.090 $cm^2\ V^{-1}\ s^{-1}$ to 0.202 $cm^2\ V^{-1}\ s^{-1}$, ascribing to a mixed electron recombination-injection process. Furthermore, the $CsPbBr_3$ nanofilm would decrease the responsivity to 136 and 178 A/W under the light wavelength of 400 and 500 nm, respectively, while decorating $CsPbBr_3$ nanoparticles improve the photoresponse to 948 and 883 A/W with the detectivity at the level of $10^{11}$ Jones. This work may provide an easy and cost-efficient way to tune the photoresponse of $MoS_2$ photodetectors.



Two-dimensional (2D) transition metal dichalcogenides (TMDCs) are promising candidates for next-generation electronic and optoelectronic devices [1–5]. As a typical member in TMDCs family, molybdenum disulfide ($MoS_2$) gains much attention due to its excellent properties, such as layer-dependent band structure, high carrier mobility and current on/off ratio [5–8]. Moreover, as the thickness decreasing to monolayer, its energy band structure evolves to direct band gap with the value of 1.8 eV. Therefore, it is widely used as photoresponse in visible. Combing the realization of the wafer-scale growth strategy, monolayer $MoS_2$ has been considered as the most promising candidate to potential application in industry [5,6,9–13].

However, the intrinsic and constant electronic structure limits the application of $MoS_2$. For example, its detection wavelength is usually in the visible range without reasonable photoresponse in near-infrared or further long wavelength. Moreover, the monolayer structure makes the light adsorption lower, thus, the photoelectrical conversation much lower. Therefore, the photoresponse is much lower in the range of mA/W. Although the gating tuning and ferroelectric tuning could suppress its dark current, as a result improve the photoresponse [6], the fabrication become much complex. Recently, surface decoration is utilized to further enhance the electric and photoelectric properties of the $MoS_2$-based devices where the introduction of additive tunes the electronic structure of $MoS_2$. For example, Cho *et al.* [14] enhanced the photocurrent of monolayer $MoS_2$ by coating PbS nano materials. Wang *et al.* [15] improved the electron concentration and source-drain current of back-gated monolayer $MoS_2$ transistor by surface charge transfer doping with black phosphorus (BP) nanoparticles. Different with PbS and BP, $CsPbBr_3$ is a typical light harvesting material in perovskite solar cells with excellent moisture and thermal stabilities [16–18]. It was applied in photodetectors with the powerful weak-light detection and ultralow dark current ($< 1$ pA) [16,19]. However, this application was limited by the slow light response due to the long charge transport distance between the two electrodes and the requirement of extra power amplifier [16,20,21].

* Corresponding author.
*E-mail address:* zegao@scu.edu.cn (Z. Wang).

https://doi.org/10.1016/j.cclet.2022.107979
1001-8417/

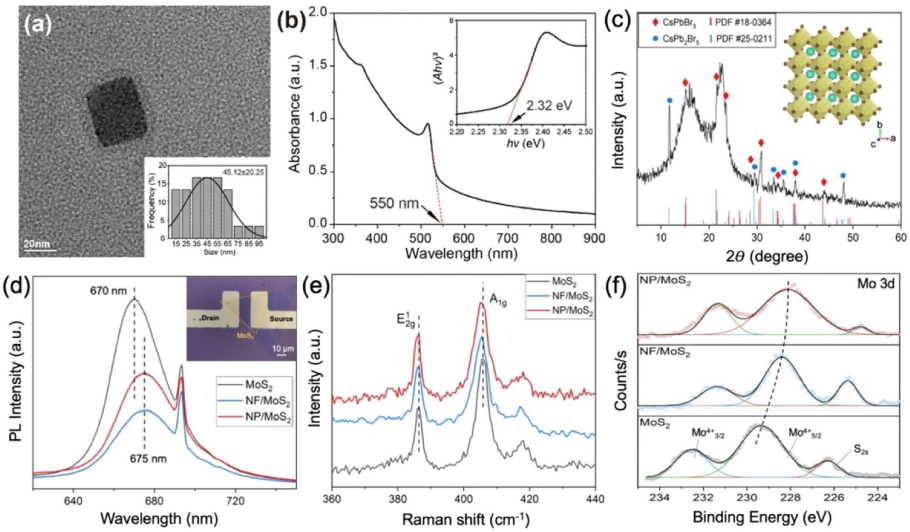


**Fig. 1.** Characterization of the $CsPbBr_3$ NPs and $MoS_2$-FET devices. (a) TEM image of the $CsPbBr_3$ NP; the inset shows the corresponding size distributions with Gaussian fits. (b) Absorption spectrum of the $CsPbBr_3$ NPs; the inset shows the Tauc plot for the corresponding absorption spectrum. (c) XRD patterns of the nanoparticle samples and the PDF cards of #18–0364 and #25–0211; the inset shows the crystal structure of the monoclinic $CsPbBr_3$. (d) PL spectra of $MoS_2$ and $CsPbBr_3/MoS_2$; the inset shows the representative optical microscope image of the $MoS_2$-FET. (e) Raman spectra of the $MoS_2$ and $CsPbBr_3/MoS_2$. (f) High-resolution XPS Mo 3d spectra of the $MoS_2$ and $CsPbBr_3/MoS_2$.

Herein, the combination of $CsPbBr_3$ and $MoS_2$ photoelectric materials was taken into consideration to achieve a photodetector with high light sensitivity, high photoelectric current and ultra-high on/off ratio. In this purpose, the $MoS_2$ phototransistor was decorated by $CsPbBr_3$ nanoparticles in two configurations, nano-film (NF) coating and nanoparticle (NP) doping. The results of the photoelectric performance investigation showed that $CsPbBr_3$ NP-doping decoration can improve the current, carrier mobility and on/off ratio of the monolayer $MoS_2$ device, which provide a potential strategy to tune the property of $MoS_2$.

Firstly, $Cs_2CO_3$ (0.065 g), octadecylene (ODE, 3 mL), and oleic acid (OA, 0.25 mL) was added to the three-neck flask. Then, the mixture was stirred and heated at 120 °C for 1 h under the nitrogen atmosphere. Finally, the Cs (oleate) solution was obtained. Simultaneously, $PbBr_2$ (0.144 g), ODE (10 mL), oleylamine (1 mL) and OA (1 mL) were added to another three-neck flask. And the mixture was heated at 105 °C for 1 h under the nitrogen atmosphere. Then the obtained Pb solution was heated to 170 °C. Next, the Cs (oleate) solution (0.9 mL) was heated to 150 °C and rapidly injected to the 170 °C Pb solution under vigorous stirring for 5 s. Subsequently, the reaction was quenched by the ice-water bath treatment. At last, the obtained product was mixed with toluene and centrifuged for 5 min to collect the sediment.

$MoS_2$ films were grown on sapphire substrate by CVD method in a two-zone tube furnace, using pre-oxidized molybdenum foil as Mo source and sulfur powder as S source. The volatilization temperature of sulfur was at 170 °C, while the Mo source was heated at 850 °C under Ar flow rate of 150 sccm for growth of $MoS_2$.

The as-grown $MoS_2$ was then transferred to the fresh $SiO_2/Si$ substrate under assistance of PMMA layer to fabricate a back-gate field effect transistor (FET). The source and drain electrodes were pre-prepared on the $SiO_2/Si$ substrate. Then the device was annealed at 250 °C for 2 h in mixed $H_2$-Ar gas before spin-coating with $CsPbBr_3$/hexane solution (1 and 0.001 mg/mL concentrations) for surface decoration. The optoelectronic property of the device was measured by a homemade vacuum probe station containing Keithley 2614B (Tektronix, US) as the source and meter. The UV–vis-NIR spectrophotometry was performed by UV-3600 (Shimadzu, Japan). The TEM images were obtained using Tecnai G2 F20S (FEI, US).

TEM image in Fig. 1a elucidates the morphology and microstructure of the $CsPbBr_3$ nanoparticles (NPs), where the inset shows the size distribution based on Gaussian fits and the average size to be $45.12 \pm 20.25$ nm. UV–vis-NIR spectrophotometry was used to investigate the optical properties of the as-synthesized NPs and the absorption spectrum of the solution-processed $CsPbBr_3$ is displayed in Fig. 1b. The absorption edge is located at about 550 nm, which is consistent with the literature [16,22]. The corresponding bandgap of the NPs is derived to be 2.32 eV from a plot of $(Ahv)^2$ *versus* $(hv)$ (inset of Fig. 1b) using Kubelka-Munk equations [16,23]. As shown in Fig. 1c, the XRD peaks at $2\theta = 15.2°$, 21.7°, 23.5°, 28.6°, 30.9°, 34.3°, 37.9° and 43.9° indicated the monoclinic phase of $CsPbBr_3$ (PDF #18–0364; the crystal structure is shown in the inset of Fig. 1c), which consists with the structure of the perovskite $CsPbBr_3$ NPs reported in literature [22,24,25]. Whilst, the phase of tetragonal $CsPb_2Br_5$ (PDF #25–0211; $2\theta = 11.7°$, 29.5°, 33.5°, 35.5°, 37.9° and 48.0°) was also observed in the XRD pattern, which might be the residuals from the $CsPbBr_3$ sample preparation. Some work [22,24,26] has reported that the $CsPb_2Br_5$ may remain in the $CsPbBr_3$ samples, because these two structures can reversibly transition under different temperatures. The inset of Fig. 1d displays the back-gate FET used in this study, which was fabricated by transferring as-grown $MoS_2$ film to the fresh $SiO_2/Si$ substrate under assistance of PMMA layer. Then two types of surface decoration with $CsPbBr_3$ perovskite were proceeded for them to turning their photoelectrical properties. One transistor was spin-coated with 1 mg/mL $CsPbBr_3$/hexane solution for a nano-film coating decoration (NF-coating). Another one was spin-coated with 0.001 mg/mL $CsPbBr_3$/hexane solution for a nanoparticles doping decoration (NP-doping). An obvious peak shift was found from the photoluminescence (PL) spectra of monolayer $MoS_2$ in Fig. 1d, which indicated an electronic band structure change for the decorating $MoS_2$ film. As seen, the pure $MoS_2$ exhibits a stronger PL intensity as compared to the NP-doped $MoS_2$, owing to its low lattice scattering [6]. Moreover, an intensity drop was observed after NF-coating, due to the unperfect $CsPbBr_3/MoS_2$ interface, which impeded the recombination of excitons, resulting in less direct band gap emission [27,28]. In addition, the sharp peak around 693 nm is for the sapphire substrate [29]. Raman spectra in Fig. 1e clearly show two typical optical vibration modes located at

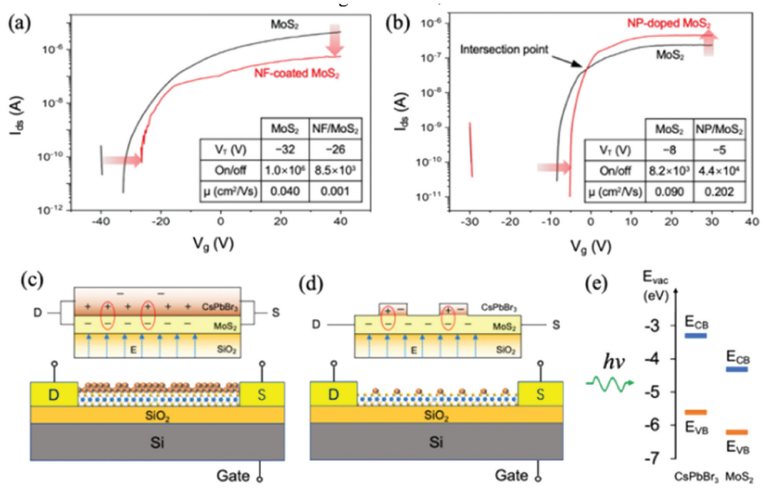


**Fig. 2.** Electrical property of $MoS_2$ and $CsPbBr_3/MoS_2$. (a, b) Transfer curves of the $MoS_2$ and $CsPbBr_3/MoS_2$ transistors; the $V_{ds}$ was fixed at 3 V. (c, d) Structure schematic of the NP-doped and NF-coated $MoS_2$ transistors. (e) The energy band diagram of $CsPbBr_3$ and monolayer $MoS_2$.

about 386 and 406 $cm^{-1}$ corresponding to the in-plane $E_{2g}{}^1$ mode and out-of-plane $A_{1g}$ mode, respectively [6]. Fig. 1f shows the high-resolution Mo 3d spectra of the as-grown and decorated $MoS_2$. C 1s peak at 284.8 eV was used for the baseline calibration [30]. The peaks of the as-grown $MoS_2$ at 232.5, 229.3 and 226.3 eV can be assigned to the signal of $Mo^{4+}$ $3d_{5/2}$, $Mo^{4+}$ $3d_{3/2}$ and S 2s, respectively [6,31,32]. It also can be seen that a distinct shift towards lower binding energy occurred after $CsPbBr_3$ decorating, which indicated the electron migration from $CsPbBr_3$ to $MoS_2$ at their interface. This mechanism is also consistent with their Fermi level [25,33].

To well reveal the tuning of $CsPbBr_3$ NPs, the electrical and photoelectrical property of $MoS_2$ device is firstly investigated, and then *in-situ* decorated with $CsPbBr_3$ NPs. Therefore, the effect of the electrode contact property can be neglect. Fig. 2 shows the surface decoration effects of NF-coating and NP-doping for the $MoS_2$-FET. It was found that the threshold voltage ($V_T$) had a slight right shift by 3–6 V after $CsPbBr_3$ decoration, as a result of the p-type $CsPbBr_3$ doping to the n-type $MoS_2$ semiconductor [6,34,35]. This shift was not sensitive to the different decorating types. However, they showed different effects on the electrical property of $MoS_2$-FET. The $I_{ds}$ of the transistor decreased by one order of magnitude at the gate voltage ($V_g$) of 40 V after NF-coating (Fig. 2a), which was mainly due to the electron-hole recombination at the interface between the $CsPbBr_3$ and $MoS_2$ [35,36]. The on/off ratio decreased from $10^6$ to $8 \times 10^3$ after NF-coating. The carrier mobility ($\mu$) decreased from 0.040 $cm^2$ $V^{-1}$ $s^{-1}$ to 0.001 $cm^2$ $V^{-1}$ $s^{-1}$ at the $\Delta V_g$ of 12 V. In addition, $\Delta V_g$ is the increment of gate voltage at the on-state current calculated by ($V_g$ – $V_T$). The $\mu$ is calculated by [37]:

$$\mu = \frac{L}{WV_{ds}C_0}\frac{dI_{ds}}{dV_g} \quad (1)$$

where $V_{ds}$ is the basis bias voltage. $C_0$ is the capacitance of the $SiO_2$. $L$ and $W$ are the channel length and width, respectively. As shown in Fig. 2c, the NF-coating decoration formed a conductive film layer on the surface of the $MoS_2$ film, which works similarly as parallel circuit in the transistor. The hole of the NF recombined with the electron of the $MoS_2$ at the interface, which reduced the electron carriers in the $MoS_2$ and decreased its electron current. According to Tong *et al.* [23,38], the defects at the interface of $CsPbBr_3$ film usually act as charge recombination centers in devices, which significantly impedes electron carrier transport. Meanwhile, the rest hole carriers still dominated the conductive NF with a decreased hole current. Thus, the total current of the transistor decreased [39]. On the other hand, the NP-doping decoration showed an improvement in conductivity (Fig. 2b), attributing to its different action principle. As shown in Fig. 2d, the 0.001 mg/mL $CsPbBr_3$ doped on the $MoS_2$ surface instead of forming a conductive layer. At first, the hole in the NPs recombined with the electron of the $MoS_2$, which led to a decrease of $I_{ds}$. As $V_g$ increases, the $I_{ds}$ of the $CsPbBr_3/MoS_2$ transistor exceeded that of the original $MoS_2$ transistor from the intersection point as shown in Fig. 2b, which was due to that the higher positive $V_g$ prompted the electron carriers of the NPs to join in the electron current in the $MoS_2$ film. This kind of surface charge transfer doping with NPs were also reported by Wood [40] and Wang [15]. Moreover, the on/off ratio increased from $8 \times 10^3$ to $4 \times 10^4$ after NP-doping, which was attributed to the higher on-state current and lower off-state current. The increase in on/off current ratio indicated an enhancement in controllability of conductive channel by $V_g$ [37]. The $\mu$ value increased from 0.090 $cm^2$ $V^{-1}$ $s^{-1}$ at the $\Delta V_g$ of 7 V to 0.202 $cm^2$ $V^{-1}$ $s^{-1}$ at the $\Delta V_g$ of 5 V, which benefits the electrical property of the device [15].

The threshold voltage ($V_T$) is the sign that the channel current ($I_{ds}$) enters on-state [37]. Fig. 3a shows the transfer curve of the NP-doped $MoS_2$ under 400 nm wavelength. It was found from Fig. 3b that the $V_T$ of both the NF-coated and NP-doped $MoS_2$ had a positive shift by 6–9 V under 400 nm wavelength, which is not sensitive to the power density. This increment of $\Delta V_g$ was suggested to be expended by the doped p-type $CsPbBr_3$ with the extracted holes [41]. Responsivity ($R$) is defined as the photocurrent induced by the excitation of unit incident laser power and detectivity ($D^*$) is defined as the capacity of the detector to detect weak light signals [42]. They can be calculated as following [37]:

$$R = \frac{I_p - I_d}{P_{opt}} \quad (2)$$

$$D^* = \frac{A^{\frac{1}{2}}R}{(2eI_d)^{\frac{1}{2}}} \quad (3)$$

where $I_p$ is the photocurrent, $I_d$ is the dark current, $P_{opt}$ is the optical power density, $A$ is the effective device area and $e$ is the electronic charge. Figs. 3c and d show the comparison of the $R$ and $D^*$ results of the $MoS_2$ and $CsPbBr_3/MoS_2$ phototransistors at various power density under wavelength of 400 nm. It was observed that the $R$ and $D^*$ of the phototransistor dropped by about seven times after NF-coating, which was suggested to due to that the photoelectric response of $MoS_2$ film was replaced by the response

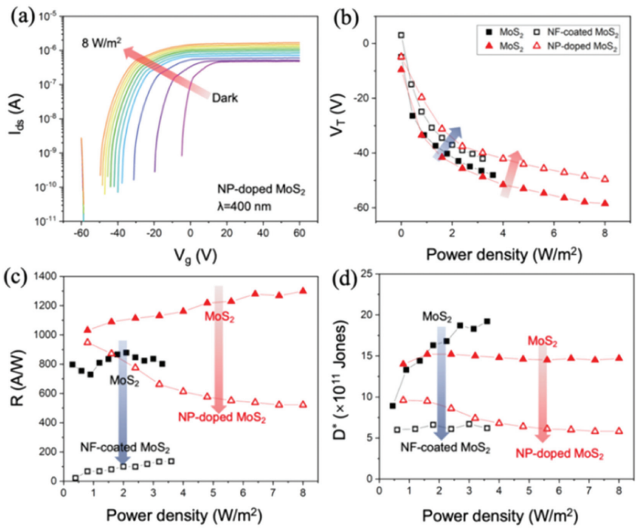


**Fig. 3.** Photoelectric property of $MoS_2$ and $CsPbBr_3/MoS_2$ phototransistors. (a) Transfer curve of the NP-doped $MoS_2$ photodetector under 400 nm wavelength. The bias voltage is fixed at 3 V. (b) Threshold voltage, (c) responsivity and (d) specific detectivity of the $MoS_2$ and $CsPbBr_3/MoS_2$ photodetectors under 400 nm wavelength with different power density.

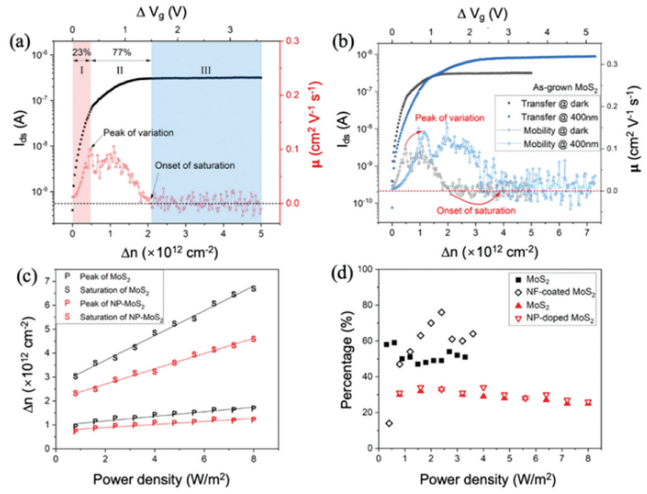


**Fig. 4.** Analysis of photoelectric performance of $MoS_2$ and $CsPbBr_3/MoS_2$ phototransistors. (a) Segmentation of the transfer and carrier mobility curves. (b) The effect of illumination on the transfer curve and carrier mobility. The power density of the 400 nm wavelength light was 1.6 W/m$^2$. The $V_{ds}$ was fixed at 3 V. (c, d) The effect of power density on the carrier concentration and mobility.

of the covered NF [38]. The larger bandgap of $CsPbBr_3$ than that of $MoS_2$ makes it harder for electrons to be excited from the valence band to the conduction band [6,22]. As the power density increased, more excited holes contributed to the photocurrent of $CsPbBr_3$, resulting in a higher photo responsivity (see the curve of NF-coated $MoS_2$ in Fig. 3c) [4]. Meanwhile, the $R$ and $D^*$ of the phototransistor show a decrease after NP-doping, which was attributed to the reduction in photocurrent caused by the recombination between the hole of $CsPbBr_3$ NPs and the electron of $MoS_2$ film. Contrary to the NF-coated $MoS_2$, the $R$ value decreased as the power density increased for NP-doped $MoS_2$, which was due to that the higher power density promotes the hole-electron recombination between the doped NPs and the $MoS_2$ film [43].

The increased electron concentration ($\Delta n$) caused by increased positive $V_g$ can be calculated by [37]:

$$\Delta n = \Delta V_g C_0 / e \tag{4}$$

where $C_0$ is the capacitance of the $SiO_2$ and $e$ is the charge. The carrier mobility ($\mu$) can be obtained from the derivation of the $I_{ds}$-$V_g$ curve, which indicates the gradient of the transfer curve. As shown in Fig. 4a, the $\mu$ curve can be divided into three regions: rise, drop and flat, corresponding to a rapid growth, slow growth and saturation of $I_{ds}$. Therefore, the three regions present the different dominant factors affecting the variation of $I_{ds}$ under a rising $V_g$. In Region I, the value of $\mu$ has a highest growth rate and the slope is higher than 1, which indicates that the increase of carrier mobility is the dominant factor for the increase of $I_{ds}$, that is, the increase of $V_g$ mainly affects $\mu$ [44]. In Region II, the value of $\mu$ decreases with increasing $V_g$. This is due to the gradually increasing carrier concentration, which increases the scattering probability in the system. $\mu$ is inversely proportional to the scattering probability [12,45]. The current in channel can be expressed as ($qnvs$), where $q$ is the electric charge, $n$ is the carrier concentration, $v$ is the electron velocity and $s$ is the cross-sectional area [44]. The electron velocity can be determined as ($\mu E$), where $E$ is the electric field. Thus, the $I_{ds}$ can be expressed as [44]:

$$I_{ds} = qn\mu Es \tag{5}$$

where $n$ and $\mu$ are the two main contributing factors for the current. As $\mu$ is decreasing, $n$ becomes the dominant contributor for the increasing $I_{ds}$ in Region II. In Region III, $I_{ds}$ becomes saturation with increasing $V_g$, where the semiconductor presents metallic property [37]. Furthermore, it was also found that its peak of variation and onset point of saturation shifted to right with higher power density (Fig. 4b), which indicates a longer lifetime of the carrier. The values of the peak and the onset point are graphed in Fig. 4c and show a linear correlation with the power density. That is, the power density can increase the carrier mobility and carrier concentration linearly, and consequently delay the time of current saturating. Fig. 4d shows the value of (Region I/(I + II) × 100%) *versus* power density, which presents the transformation of dominant factor affecting the $I_{ds}$. The I/(I + II) value of phototransistor decreased slightly with increasing power density, which indicates that the increasing power density would enhance the increment of $\mu$ under increasing $V_g$. The value of NP-doped $MoS_2$ shows a similar curve trend with a higher I/(I + II) value. That is, the NP-doping can benefit the carrier mobility, which may be attributed to the lower scattering of electron [45,46]. However, the NF-coated $MoS_2$ threw off the trend of I/(I + II) value, as a result of the compilated combination of the $CsPbBr_3$ and $MoS_2$ phototransistors.

Fig. 5 exhibits the photoelectric properties of $MoS_2$ and $CsPbBr_3/MoS_2$ phototransistors under different wavelength of 400, 500 and 700 nm. As shown in Fig. 5b, NF-coating made the R of $MoS_2$ decreased from 878, 1838 and 833 A/W to 136, 178 and 367 A/W, which was attributed to the recombination between the p-type $CsPbBr_3$ NF and the n-type $MoS_2$ film. Moreover, the photoelectric response of $CsPbBr_3$ layer consumed part of the light energy without a significant photoelectric response and weakened the light for $MoS_2$ film. Also, defects of the interface would restrict the electron mobility [43]. The $R$ of the NP-doped $MoS_2$ decreased from 1299, 1645 and 647 A/W to 948, 883 and 413 A/W, due to the recombination between the photogenerated hole of the doped NPs and the photoelectron of the $MoS_2$. Meanwhile, the $D^*$ value remains at $10^{11}$ Jones after NF-coating and NP-doping. Figs. 5e and f show the rise and fall time of the photoelectric response at wavelength of 400, 500 and 700 nm. The rise (fall) time is defined as the time-resolved photocurrent increases (decreases) from 10% to 90% (90% to 10%) of the maximum photocurrent [37], which was measured under the fixed $V_g$ at $V_{ds}$ of 5 V. It was found that the NF-coating extended both the rise and fall time for $MoS_2$, which was caused by the shield of the $CsPbBr_3$ layer over the $MoS_2$ film. However, the NP-doping did not impact the photoresponse speed significantly.

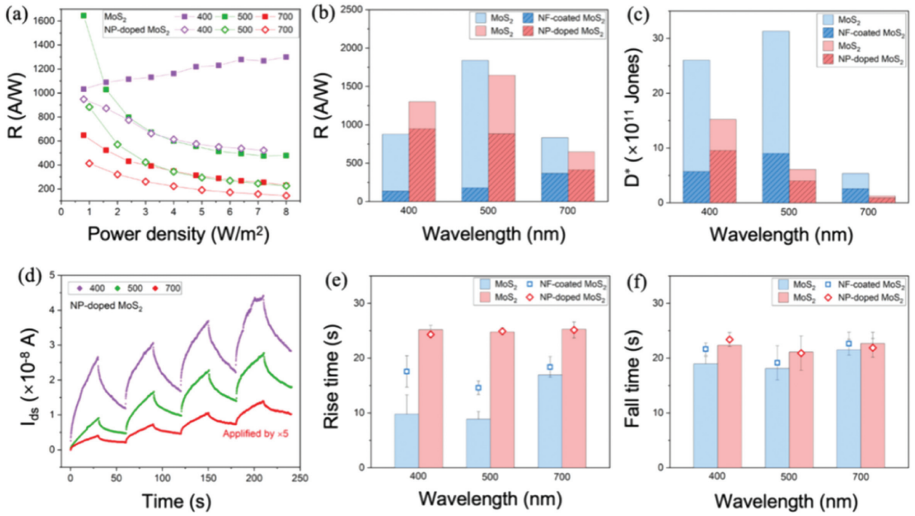


**Fig. 5.** Photoelectric property of $MoS_2$ and $CsPbBr_3/MoS_2$ phototransistors under different wavelengths. (a) The maximum responsivity of the $MoS_2$ and $CsPbBr_3$ NP-doped $MoS_2$ with increasing illumination power density under different wavelengths at a gate voltage range of −60~60 V. (b, c) Responsivity and specific detectivity of the $MoS_2$ and $CsPbBr_3/MoS_2$ photodetectors under different wavelengths. (d) Time-resolved photoresponse of the $MoS_2$ and $CsPbBr_3$ NP-doped $MoS_2$ under different wavelengths. (e, f) Rise and fall time of the $MoS_2$ and $CsPbBr_3/MoS_2$ photodetectors under different wavelengths. The bias voltage is fixed at 3 V.

In summary, $CsPbBr_3$ nanoparticles were used to decorate the $MoS_2$ FET *via* NF-coating and NP-doping methods separately. It was found that the conductivity, carrier mobility and on/off current ratio of the monolayer $MoS_2$ were significantly improved after $CsPbBr_3$ NP-doping, which was suggested to due to a mixed electron recombination-injection process. Furthermore, it was found that nanofilm-coating of $CsPbBr_3$ would impede the photoelectric performance due to the electron-hole recombination facilitated by the defects at the interface of $CsPbBr_3$ and $MoS_2$ films. By decorating with $CsPbBr_3$ nanoparticles, the photoresponse of $MoS_2$ transistor could improve to 948 and 883 A/W at 400 nm and 500 nm illumination, and the detectivity can rise to about $10^{11}$ Jones. This work may provide an easy and cost-efficient way to tune the photoresponse of $MoS_2$ photodetectors.

## Declaration of competing interest

The authors declare that they have no known competing financial interests or personal relationships that could have appeared to influence the work reported in this paper.

## Acknowledgmnts

This work was financially supported by the National Natural Science Foundation of China (Nos. 52002254, 52272160), Sichuan Science and Technology Foundation (Nos. 2020YJ0262, 2021YFH0127, 2022YFH0083, 2022YFSY0045), the Chunhui plan of Ministry of Education, Fundamental Research Funds for the Central Universities, China (No. YJ201893), the Open-Foundation of Key Laboratory of Laser Device Technology, China North Industries Group Corporation Limited (No. KLLDT202104) and Supported by the fund of the State Key Laboratory of Solidification Processing in NWPU (No. SKLSP202210).

## References

[1] X. Song, J. Xu, L. Liu, et al., Appl. Surf. Sci. 542 (2021) 148437.
[2] J. Wang, X. Xu, T. Cheng, et al., Nat. Nanotechnol. 17 (2022) 33–38.
[3] H. Huang, J. Zha, S. Li, et al., Chin. Chem. Lett. 33 (2022) 163–176.
[4] X. Niu, Y. Yu, J. Yao, et al., Chem. Phys. Lett. 772 (2021) 138571.
[5] D.S. Schneider, A. Grundmann, A. Bablich, et al., ACS Photonics 7 (2020) 1388–1395.
[6] X. Luo, Z. Peng, Z. Wang, et al., ACS Appl. Mater. Interfaces 13 (2021) 59154–59163.
[7] M. Liao, Z. Wei, L. Du, et al., Nat. Commun. 11 (2020) 2153.
[8] L. Wang, X. Li, C. Pei, et al., Chin. Chem. Lett. 33 (2022) 2611–2616.
[9] S. Luo, C.P. Cullen, G. Guo, et al., Appl. Surf. Sci. 508 (2020) 145126.
[10] R. Muñoz, E. López-Elvira, C. Munuera, et al., Appl. Surf. Sci. 581 (2022) 151858.
[11] J. Zha, M. Luo, M. Ye, et al., Adv. Funct. Mater. 32 (2022) 2111970.
[12] L. Bu, Y. Qiu, P. Wei, et al., Phys. Rev. Appl. 6 (2016) 054022.
[13] C. Zhu, I. Ahmed, A. Parsons, et al., Polym. Compos. 39 (2018) 140–151.
[14] S. Cho, Y. Jo, H. Woo, et al., Appl. Sci. Converg. Technol. 26 (2017) 47–49.
[15] W. Wang, X. Niu, H. Qian, et al., Nanotechnology 27 (2016) 505204.
[16] X. Liu, Z. Liu, J. Li, et al., J. Mater. Chem. C 8 (2020) 3337–3350.
[17] H. Min, D.Y. Lee, J. Kim, et al., Nature 598 (2021) 444–450.
[18] R. Lin, J. Xu, M. Wei, et al., Nature 603 (2022) 73–78.
[19] W. Zhai, J. Lin, C. Li, et al., Nanoscale 10 (2018) 21451–21458.
[20] Y. Li, Z.F. Shi, S. Li, et al., J. Mater. Chem. C 5 (2017) 8355–8360.
[21] Y. Meng, C. Lan, F. Li, et al., ACS Nano 13 (2019) 6060–6070.
[22] J. Duan, Y. Zhao, B. He, et al., Angew. Chem. Int. Ed. 57 (2018) 3787–3791.
[23] G. Tong, T. Chen, H. Li, et al., Nano Energy 65 (2019) 104015.
[24] K. Du, L. He, S. Song, et al., Adv. Funct. Mater. 31 (2021) 2103275.
[25] K.C. Tang, P. YouF. Yan, Sol. RRL 2 (2018) 1800075.
[26] F. Palazon, S. Dogan, S. Marras, et al., J. Phys. Chem. C 121 (2017) 11956–11961.
[27] J. Choi, H. ZhangJ. H. Choi, ACS Nano 10 (2016) 1671–1680.
[28] H. Ahn, Y.C. Huang, C.W. Lin, et al., ACS Appl. Mater. Interfaces 10 (2018) 29145–29152.
[29] T. Han, H. Liu, S. Wang, et al., Nanomaterials 9 (2019) 740.
[30] C. Tan, C.D. Rudd, A.J. Parsons, et al., J. Mech. Behav. Biomed. Mater. 136 (2022) 105480.
[31] A. Syari'ati, S. Kumar, A. Zahid, et al., Chem. Commun. 55 (2019) 10384–10387.
[32] C.K. Cheng, C.H. Lin, H.C. Wu, et al., Nanoscale Res. Lett. 11 (2016) 117.
[33] X. Pan, M. Yan, C. Sun, et al., Adv. Funct. Mater. 31 (2020) 2007840.
[34] J. Liu, F. Liu, H. Liu, et al., Nano Today 36 (2021) 101055.
[35] T. Qin, Z. Wang, Y. Wang, et al., Nano-Micro Lett. 13 (2021) 183.
[36] B. Cao, Z. Ye, L. Yang, et al., Nanotechnology 32 (2021) 412001.
[37] F. Li, R. Tao, B. Cao, et al., Adv. Funct. Mater. 31 (2021) 2104367.
[38] G. Tong, H. Li, D. Li, et al., Small 14 (2018) 1702523.
[39] D. Wang, Z. Wang, Z. Yang, et al., Mater. Today Phys. 24 (2022) 100678.
[40] J.D. Wood, S.A. Wells, D. Jariwala, et al., Nano Lett. 14 (2014) 6964–6970.
[41] W. Chen, K. Li, Y. Wang, et al., J. Phys. Chem. Lett. 8 (2017) 591–598.
[42] L. Hao, Y. Du, Z. Wang, et al., Nanoscale 12 (2020) 7358–7365.
[43] C. Chen, Y. Wu, L. Liu, et al., Adv. Sci. 6 (2019) 1802046.
[44] X.F. Zhang, L. Wei, L. Wang, et al., Appl. Phys. Lett. 102 (2013) 113501.
[45] D.B. Farmer, R. Golizadeh-Mojarad, V. Perebeinos, et al., Nano Lett. 9 (2009) 388–392.
[46] R. Tao, Z. Hao, C. Tan, et al., J. Electron. Sci. Technol. 20 (2022) 100167.